Journal of Nuclear Materials 377 (2008) 522–527

Contents lists available at ScienceDirect

Journal of Nuclear Materials

journal homepage: www.elsevier.com/locate/jnucmat

Grain boundary influence on displacement cascades in UO_2: A molecular dynamics study

L. Van Brutzel [a,*], E. Vincent-Aublant [b]

[a] CEA-Saclay, DEN/DPC/SCP, bâtiment 450 Sud, 91191 Gif-Sur-Yvette, France
[b] CEA-Valrhô, DEN/DTCD/SECM, bâtiment Atalante, 30207 Bagnols-Sur-Cèze, France

ARTICLE INFO

Article history:
Received 4 March 2008
Accepted 17 April 2008

PACS:
61.72.Mm
61.80.Lj
61.82.Rx

ABSTRACT

The influence of grain boundaries on the primary damage state created by a recoil nucleus in UO_2 matrix is studied here by molecular dynamics simulations. This study is divided in two steps: (1) the study of the structural properties of several symmetrical tilt boundaries for different misorientation angles ranging from 12.7° to 61.9°; and (2) the study of displacement cascades near these grain boundaries. For all the grain boundaries studied, the structure around the interface up to about 2 nm presents a perturbed but stable fluorite lattice. The type of defect at the interface depends directly on the value of the misorientation angles. For the small angles (12.7° and 16.3°) the interface defects correspond to edge dislocations. For higher misorientation angles, a gap of about 0.3 nm exists between the two halves of the bicrystal. This gap is composed of Schottky defects involving numerous vacancies along the interface. About 10 keV displacement cascades were initiated with an uranium projectile close to the interface. In all the cases, numerous point defects are created in the grain boundary core, and the mobility of these defects increases. However, cascade morphologies depend strongly on the grain boundary structure. For grain boundaries with edge dislocations, the evolution of the displacement cascades is similar to those carried out in monocrystals. On the other hand, cascades initiated in grain boundaries with vacancy layer defects present an asymmetry on the number of displaced atoms and the number of point defects created.

1. Introduction

Uranium dioxide (UO_2), the main component of the present nuclear fuel, undergoes during its lifetime in a reactor, and subsequently in storage, numerous radiations and structural changes. In order to better characterize its long term behavior and understand alterations of its physical properties, a basic knowledge of physical phenomena which create structural damage at the atomic scale is essential. The analysis of nanometric defects is not easily accessed experimentally due to the defect length scale and the irradiation events timescale. Atomistic simulation is then a suitable alternative providing insight into atomic structure and damage mechanisms.

Previous simulations of collision cascade sequences which reproduce the primary damage state created by a recoil nucleus were carried out in UO_2 with empirical interatomic potential molecular dynamics (MD) [1,2]. These simulations reveal no amorphization of the matrix even for high energies of the initial projectile (up to 80 keV) or cascade overlaps in agreement with experimental observations [3–5]. Only few point defects are created with mainly vacancies located in the cascade's core and interstitials distributed at the periphery of the sub-cascade branches. Up to now, all these previous simulations have been carried out in monocrystals. However, real nuclear fuels are made of several UO_2 crystals of different sizes separated by interfaces or grain boundaries (GBs). It is well-known that these GBs, considered as interfacial defects, influence the mechanical and the physical properties. For instance, they could act as sinks for the defects, which increase the material resistance under irradiation. Few numerical studies have been carried out on the subject and are mainly concentrated on metallic systems [6,7]. Moreover, impact of GBs on the creation or annihilation of point defects as well as their role on the transport properties are yet still unclear in the case of UO_2.

In general GBs are complex structures involving a multitude of different orientations and sizes. However, simple geometries, like symmetrical tilt boundaries presented herein, give some insight of how GB affect the creation of point defects under irradiation. In this article we will present the study of displacement cascades initiated close to GBs. This study has been done in two steps. First, the analysis of the atomic structure and relaxation of several tilt GBs for different misorientation angles is carried out in UO_2 bicrystals. Although geometric [8,9] and bicrystallographic [10] models can be applied to all crystals, the specific GB structure depends

* Corresponding author. Tel.: +33 1 69 08 79 15; fax: +33 1 69 08 92 21.
E-mail address: laurent.vanbrutzel@cea.fr (L.V. Brutzel).

0022-3115/$ - see front matter © 2008 Elsevier B.V. All rights reserved.
doi:10.1016/j.jnucmat.2008.04.010

strongly on the nature of chemical bonds and the crystal structure. Therefore, a specific understanding of the GB relaxation and structure in UO_2 is still necessary. The second step of the study consists of analyzing displacement cascades initiated near the interfaces of the different symmetrical tilt boundaries studied.

2. Computational procedure

MD simulations were carried out using a Born–Mayer–Huggins like potential for the repulsive part coupled with a full Ewald summation to describe the Coulomb interactions. The analytical function of the potential is defined as:

$$V_{\alpha\beta}(r_{ij}) = A_{\alpha\beta}\exp\left(-\frac{r_{ij}}{B_{\alpha\beta}}\right) - \frac{C_{\alpha\beta}}{r_{ij}^6} + \frac{z_\alpha z_\beta}{4\pi\epsilon_0 r_{ij}}, \quad (1)$$

where A, B and C are adjustable parameters, r_{ij} is the distance between the atoms i and j, z is the ionic partial charge and α and β design the type of atom. Details of the potential parameters and validation were reported by Morelon et al. [11].

A GB is defined as an interface between two monocrystals in a polycrystal. Numerous different geometries can then be created. The geometry of a GB interface can be characterized by five macroscopic degrees of freedom: the rotation axis of the crystal along the unit vector $\hat{n}$; the misorientation angle θ between both crystals; and the three components of the normal vector $\hat{n}_{GB}$ perpendicular to the interface plane. Fig. 1 represents a projection along the [001] tilt axis of a (310) symmetrical tilt boundary with a misorientation angle equal to $\theta = 36.87°$ (noted (310)/[001]Σ5). By convention we define the three Cartesians axis as: the direction perpendicular to the interface (X); the direction perpendicular to the normal vector $\hat{n}_{GB} = [310](Y)$; and the direction parallel to the unit vector $\hat{n} = [001](Z)$.

In our simulations, the GB interfaces created at the beginning of the simulation are constructed as follows: a conventional fluorite UO_2 crystal is rotated with an angle equal to $\theta/2$ on one half of the simulation box along a rotation axis perpendicular to the normal plane. The second crystal is then constructed from the first one by specular inversion with respect to the interface plane. This method of construction leads to overlap the atoms along the interface. Moreover, the periodic boundary conditions double the number of interfaces and then duplicate the problem. To solve this difficulty the interface atoms of one of the crystals are removed conserving the total box charge neutrality.

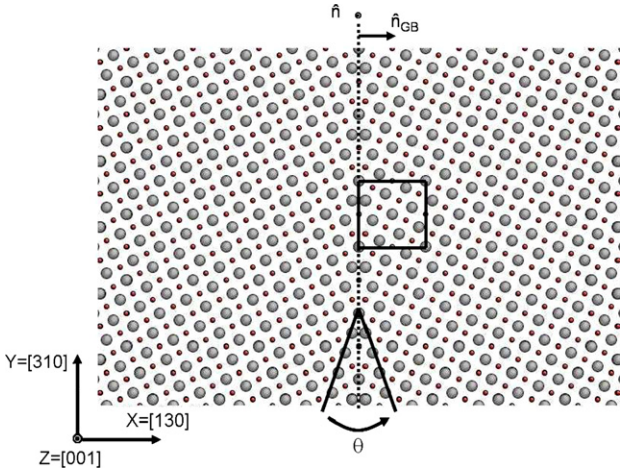

Fig. 1. Projection onto the [001] tilt direction of the symmetrical grain boundary (310)/[001]Σ5 with a misorientation angle equal to $\theta = 36.87°$. The biggest spheres represent the uranium atoms and the smallest ones the oxygen atoms. The Σ5 unit cell lattice is underlined by the square frame and the interface is underlined by the dashed line.

Most of the polycrystalline matrices in nature are formed by numerous grains slightly misoriented from one to another. In order to have a broader picture of all possible geometries, we studied six symmetrical tilt GBs with misorientation angles ranging from 12.68° to 61.92°. One of the means to characterize these geometries is to refer to the coincidence site lattice (CLS) which is the lattice of common sites for both crystals. In the following article, each GB will be referred by Σ followed by its coincidence frequency number (for instance Σ5 for the GB with a misorientation angle equal to 36.87°). Table 1 presents the notation and features of each of the six GBs studied.

For all the GBs studied, the same creation procedure has been applied. Each Σ has its own GB unit cell lattice, hence the size of each box is different. Nevertheless, for each Σ the box cubic shape is kept with sizes close to $16 \times 16 \times 16$ nm. Details of the box dimensions and the total number of atoms are presented in Table 1. After creating the GB interface, the system is relaxed for 50000 time steps under a constant temperature (300 K) and constant pressure (0 GPa) algorithm. Afterward, the system is relaxed under constant temperature and constant volume during 20000 time steps. The analysis of the structure and the calculation of the physical quantities are done during this last relaxation.

3. GB structure and energy analysis

3.1. Structure and morphology of (310)/[001]Σ5

The Σ5 symmetrical tilt GB is one of the most studied geometries experimentally as well as theoretically. In particular, several studies exist on fluorite-like structures such as yttria-stabilized cubic-zirconia [12–15]. Hence, the Σ5 geometry was chosen in order to compare our results with available data.

First the stability of the interface was investigated as well as its structure. At the end of the first relaxation, the volume of the box increases by about 4.5% while the tetragonal shape is conserved. This increase in volume is due to the formation of a gap of 0.3 nm between the two halves of the bicrystal. The comparison of the interface structure at the beginning of the simulation and at the end of the relaxation is shown in Fig. 2(a) and (b), respectively.

Comparing both pictures (Fig. 2(a) and (b)), the general structure of the interface seems to be conserved with a repetition of a triangular-like pattern (depicted by dashed lines in the figure). However, in Fig. 2(b), the distance between the two crystals has increased by about 0.3 nm. This gap is even more visible in the projection onto the (X,Z) plane at the bottom of Fig. 2(b). In this plane we can define a region where atoms have been displaced from their initial position and where the regular crystalline order

Table 1
Notation, misorientation angles and features of the simulation boxes for the different symmetrical tilt GBs studied

CLS Notation	Misorientation angle	Nomenclature	Box size [nm]	Total number of atoms
Σ41	12.68°	(910)/[001]Σ41	$19.81 \times 19.81 \times 19.6.8$	472320
Σ25	16.26°	(710)/[001]Σ25	$15.46 \times 15.46 \times 16.4$	268800
Σ13	22.61°	(510)/[001]Σ13	$16.73 \times 16.73 \times 16.4$	336960
Σ5	36.87°	(310)/[001]Σ5	$17.29 \times 17.29 \times 16.4$	360000
Σ29	46.39°	$(\bar{7}\,\bar{3}0)/[001]$Σ29	$16.66 \times 16.66 \times 16.4$	334080
Σ17	61.92°	$(\bar{5}\,\bar{3}0)/[001]$Σ17	$15.94 \times 15.94 \times 16.4$	306000

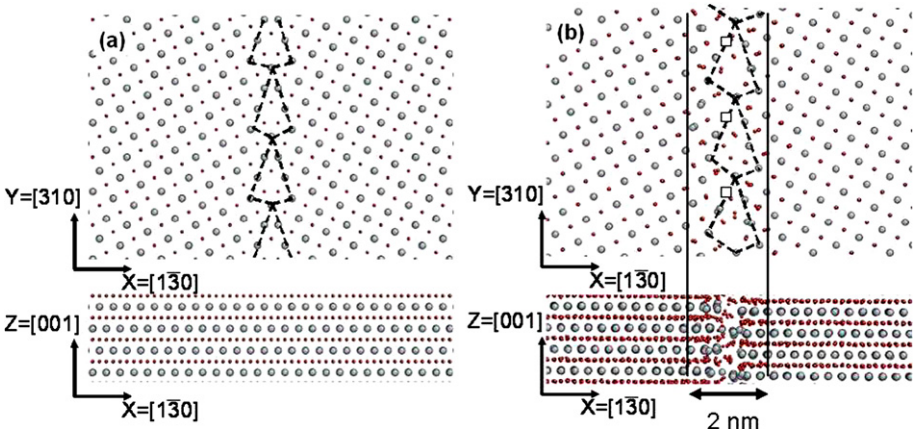

Fig. 2. Projection onto the (X,Y) plane (tops) and onto the (X,Z) plane (bottoms) both perpendicular to the GB $(3\,1\,0)/[0\,0\,1]\Sigma5$ at (a) the beginning of the simulation and at (b) the end of the relaxation. The triangular-like pattern at the interface is underlined by dashed lines. The two straight lines in (b) represent the limit of the GB core region. The squares in (b) show the localization of uranium vacancies.

is perturbed. The perturbed region is equal to about 2 nm in the bicrystal and is defined as the GB core or GB width. Furthermore, the two crystals slid relative to one another along the *Y* axis (parallel to the GB plane). This sliding which occurs during the relaxation process, destroys the mirror symmetry and creates a layer of vacancy defects. The defects are along the interface and contain 2 oxygen vacancies per 1 uranium vacancy hence giving a Schottky defect. Here, one needs to specify that it is the sliding of one crystal from the other, namely the geometrical construction alone, which creates these vacancy defects. No hop of single atom has been observed. Part of this defect layer is visible from a projection on the (X,Y) plane (top of the Fig. 2(b)) on the uranium sub-lattice. At the end of the relaxation, the triangular-like pattern involves 7 uranium atoms and one uranium vacancy, represented by a square in the Fig. 2(b), while at the beginning it is composed of 8 uranium atoms. This type of relaxation has also been observed by Fisher and Matsubara [16] and confirmed by TEM observations on Σ5 GB in yttria-stabilized cubic-zirconia [12,13]. Moreover, this triangular-like structure is similar to those predicted for fcc metals such as copper[17] except the introduction of vacancies which in the case of the ionic systems reduces the atomic repulsion. This similarity comes from the fact that UO_2 can be considered as a uranium fcc lattice with oxygen atoms filling the tetrahedral sites.

Another way to confirm the hypothesis of this sliding relaxation is to determine the evolution of the box energy as a function of the translation of one crystal to the other along the *Y* axis. An optimum exists for the translation vector in which the energy of the box is minimum. Fig. 3 represents the average potential energy of atoms within the 2 nm GB core as a function of the translation vector. The translation vector is normalized to the lattice parameter. The minimum energy corresponds to a translation vector equal to 0.8 (i.e. in the case of Σ5 to a distance equal to 0.172 nm). The configuration for this translation, see Fig. 4, corresponds to the same structure found after relaxation (Fig. 2(b)).

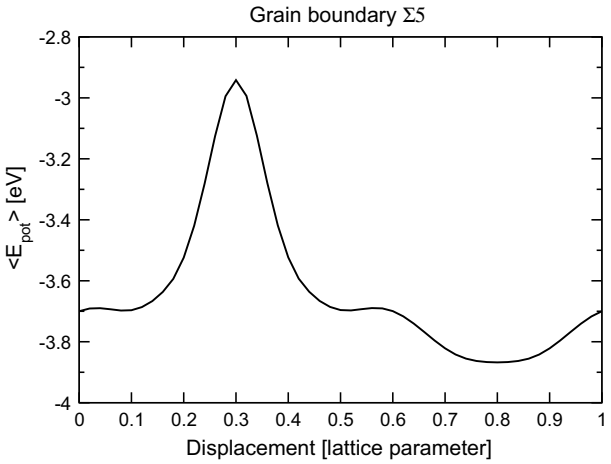

Fig. 3. Plot of the average potential energy in the GB core region as a function of the translation vector along the *Y* axis.

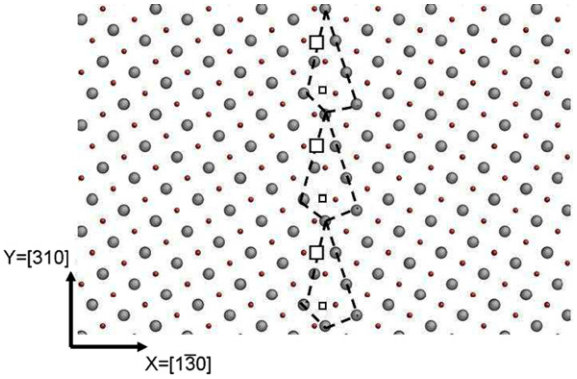

Fig. 4. Projection onto the (X,Y) plane perpendicular to the GB of the symmetrical tilt $(3\,1\,0)/[0\,0\,1]\Sigma5$ for the configuration corresponding to the minimum energy at a translation vector equal to 0.8. The big spheres and big squares represent the uranium atoms and the uranium vacancies respectively. The small spheres and small squares represent the oxygen atoms and the oxygen vacancies respectively. The dashed lines underline the triangular-like pattern at the GB interface.

3.2. Structure of other GBs

We will briefly describe the structure of the other GBs studied. All the GBs were created with the same method described in Section 2. In all the cases during the relaxation the two crystals move slightly away from each other before sliding parallel to the interface. However, the final structure of each GB cores is different. For the GBs with small misorientation angles (12.68° and 16.26°), corresponding to Σ41 and Σ25, respectively, the final structure is characterized by a line of edge dislocations with a Burgers vector equal to 0.273 nm $(a/2)$ in the $[1\,0\,0]$ direction.

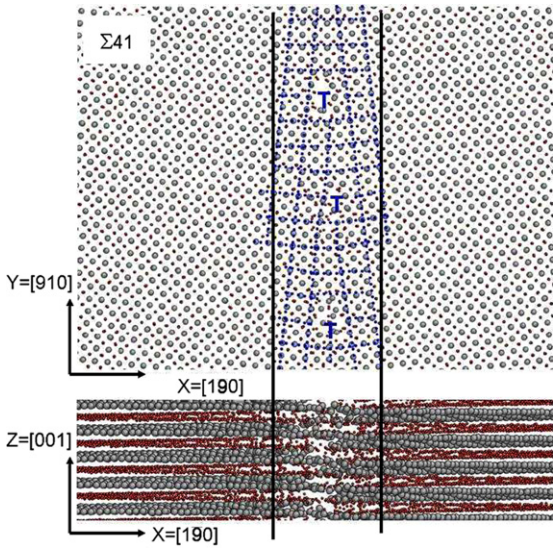

Fig. 5. Projection onto the (X,Y) plane (top) and onto the (X,Z) plane (bottom) both perpendicular to the GB (9 1 0)/[0 0 1]Σ41. The big spheres represent the uranium atoms and the small spheres the oxygen atoms. The two straight lines represent the limit of the GB core region. Dashed lines underline the conventional fluorite lattice. Edge dislocations are visible at the interface.

For illustration, Fig. 5 (top) represents the projection onto the [0 0 1] tilt axis of the Σ41 symmetrical tilt boundary. The distance between two dislocations has been measured equal to 2.45 nm and 1.99 nm for Σ41 and Σ25, respectively. These distances are approximately identical to the theoretical distance given by the following equation:

$$d = \frac{b}{\sin\frac{\theta}{2}}, \tag{2}$$

where b is the Burgers vector value (equal here to 0.273 nm) and θ the misorientation angle. Applying this equation, the theoretical calculated distance for Σ41 is 2.47 nm and for Σ25 is 1.93 nm. Hence our calculated values are in agreement with the theoretical values.

GBs with bigger misorientation angles have no particular structural pattern (excepted the triangular-like pattern for Σ5). However, numerous point defects and more specifically numerous vacancies are found at the interfaces.

3.3. GB energies

In the previous section, we described qualitatively the GB structure close to the interface and defined visually a GB core. We will now describe quantitatively the GB width. The definition is based on the potential energy differences between atoms in the bulk and atoms at the interface. Indeed, atoms close to the interface have a significantly higher potential energy than the bulk atoms due to different coordination numbers. Average cohesive energies in the bulk are −7.9 eV for the uranium atoms and −2.2 eV for the oxygen atoms. If the atomic potential energy varies by more than ±0.05 eV of the average potential energy, then the atom is considered to be part of the GB core; hence defining the GB width.

Fig. 6 represents the average potential energy of uranium atoms as a function of their distances to the interface. Here, it is important to remind the reader that due to the periodic boundary conditions two interfaces are created in the box. The GB width is equal to about 2 nm for both interfaces which is coherent with the values found qualitatively.

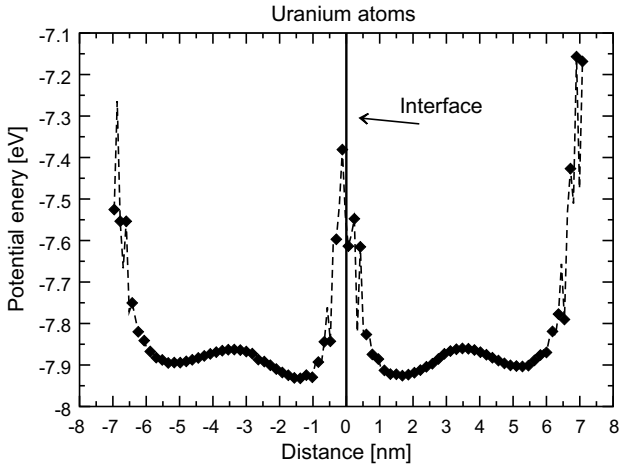

Fig. 6. Average potential energy of uranium atoms per slab of 0.1 nm width along the X axis perpendicular to the interfaces as a function of the distance from the central interface.

The GB energy per surface area, γ, is defined as the energy needed to create the GB. It is calculated as follows:

$$\gamma = \frac{\langle E_{GB}\rangle - \langle E_{bulk}\rangle}{A}, \tag{3}$$

where $\langle E_{GB}\rangle$ is the average potential energy of atoms in the GB core, $\langle E_{bulk}\rangle$ is the average potential energy of the atoms in the bulk, and A is the GB surface area. All the values of the studied GBs are gathered in Fig. 7. Excepted for Σ5, the energies are increasing with the misorientation angles. The energy for Σ5 is significantly lower than the others (1.29 J/m^2) which leads to conclude that it is the most favorable symmetrical tilt GB structure.

4. Displacement cascades

In this section, we present the results of displacement cascades near GBs. All the cascades have been carried out with the same method. Each cascades has been initiated after the relaxation phase described in the previous section. Consecutively, an uranium atom (i.e. the PKA, Primary Knock-on-Atom) which is at 3.5 nm from the interface of one of the crystals is accelerated. The system is then relaxed under constant volume. The temperature of a 0.3 nm width layer at the boundaries of the simulation box is

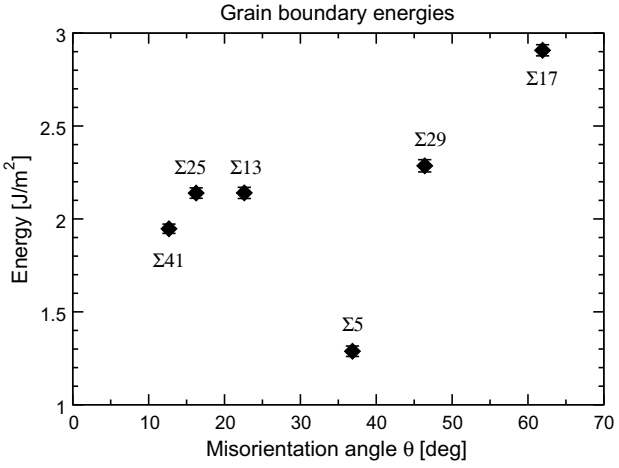

Fig. 7. GB energy per surface area as a function of the misorientation angles.

maintained at 300 K by rescaling the atom velocities in order to evacuate the excess of energy brought by the PKA. At the end of the cascade an analysis is run to determine the number and the localization of the point defects created. This analysis is done by comparing the initial atomic positions with the final atomic positions. A vacancy is then defined as an empty crystallographic site, and an interstitial is defined as an atom occupying a different position than one of the initial crystallographic site. In the case of UO_2 no dumbbell has been found. With these defect definitions, the intrinsic defects present at the interface at the beginning of the cascade are not taken into account. From previous studies of displacement cascades in UO_2 monocrystal, it has been stated that the initial direction of the PKA has no influence on the cascade morphology [1,2]. Therefore, all the PKAs were accelerated in the perpendicular direction and toward the interface. The initial PKA energy has been set to 10 keV for all simulations. This energy is sufficient to describe important physical mechanisms which take place during displacement cascades. Because the Σ5 GB seems the most favorable structure, in order to increase the statistics, 10 cascades have been carried out with this geometry with different initial PKA positions. For the other GBs, only one cascade has been carried out.

Fig. 8 shows a sequence of snapshots during a cascade initiated with a 10 keV PKA in a monocrystal (i.e. no GB). The atoms plotted in the figure are atoms which are displaced by more than 0.2 nm from their original position. The cascade morphology is quasi-spherical with some sub-cascade branches. A thermal spike occurs at about 1.125 ps (Fig. 8(c)) when the highest number of atoms are displaced.

Fig. 9 depicts snapshots of a cascade initiated in the left crystal at 3.5 nm from a Σ25 GB. The cascade morphology is spherical and a thermal spike occurs at about 1.125 ps as well. The main difference is that a large proportion of displaced atoms are concentrated around the GB.

Fig. 10 shows snapshots of a cascade initiated in the left crystal at 3.5 nm from a Σ5 GB. Once again a large proportion of displaced atoms are centerlined around the interface. This result can be explained by the presence of numerous vacancies along the interface which trap interstitials. However, in the case of Σ5 an asymmetry of displaced atoms with respect to the interface appears (Fig. 10(b)–(d)). More atoms are displaced in the left crystal. Thus, the GB containing the Schottky defects seems to act like a defect sink and prevents atoms from moving across the GB interface. Hence, only at the beginning of the cascade, when atoms have still enough kinetic energy, crossing can take place and provokes sub-cascades in the second crystal on the right.

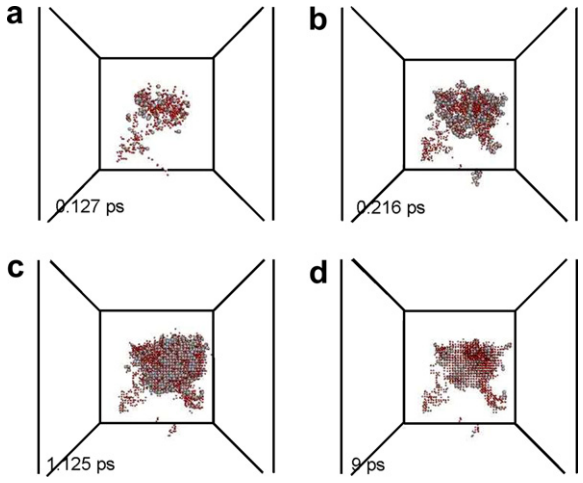

Fig. 8. Snapshots of displaced atoms during a cascade initiated with an energy of 10 keV in a monocrystal.

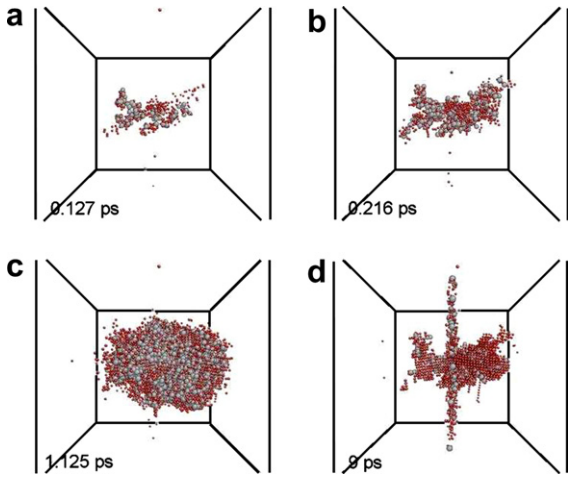

Fig. 9. Snapshots of displaced atoms for a cascade initiated with an energy of 10 keV at 3.5 nm from the interface in a symmetrical tilt (7 1 0)/[0 0 1]Σ25. The interface is located in the middle of the box.

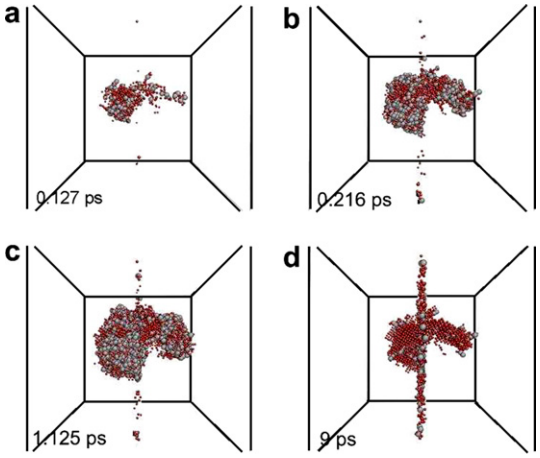

Fig. 10. Snapshots of displaced atoms for a cascade initiated with an energy of 10 keV at 3.5 nm from the interface in a symmetrical tilt (3 1 0)/[0 0 1]Σ5. The interface is located in the middle of the box.

Table 2 gives the numbers of the displaced atoms and the point defects created at the end of the cascades in a monocrystal and for all the GB geometries. For each GB the total number as well as the number in the core region are given. For the monocrystal and for the Σ5 GB, results are averaged over 10 different cascades. More atoms are displaced in bicrystals, 3873, rather than 2409 in the monocrystal. These extra displaced atoms are located mainly in the GB core, as shown in Figs. 9 and 10. Furthermore, the displacements at the GBs have been observed to be mainly parallel to the interface along the defects lines: either dislocations for small misorientation angles either vacancy lines for higher angles.

The number of point defects created at the end of cascades in bicrystal is significantly different than in monocrystal. On average, there are seven times more point defects created in bicrystals than in monocrystal and about three fourth of them are located in the GB core region. Here, one needs to recall that the initial defects located at the GB are not taken into account in this calculation. The defects found are either created or displaced during the cascade. It is also important to note that the total number of interstitials and the total number of vacancies are identical for the same cascade.

Table 2
Number of displaced atoms and point defects at the end of the cascade initiated with energies equal to 10 keV

	Displaced atoms		U vacancies		U interstitials		O vacancies		O interstitials	
	Total	GB core	Total	GB core	Total	GB core	Total	GB core	Total	GB core
Monocrystal	2409 ± 147	NA	21 ± 4	NA	21 ± 4	NA	84 ± 12	NA	84 ± 12	NA
Σ41	4065	1093	187	100	187	142	693	407	693	484
Σ25	3937	1011	127	95	127	107	629	466	629	494
Σ13	4121	1425	202	174	202	191	993	908	993	939
Σ5	3267 ± 294	1076 ± 497	116 ± 28	88 ± 26	116 ± 28	75 ± 23	437 ± 75	342 ± 53	437 ± 76	365 ± 54
Σ29	3675	1401	166	129	166	145	739	584	739	626
Σ17	4178	1400	213	167	213	188	958	747	958	806

In the case of the monocrystal and Σ5 the results presented are the average values calculated over 10 different cascades.

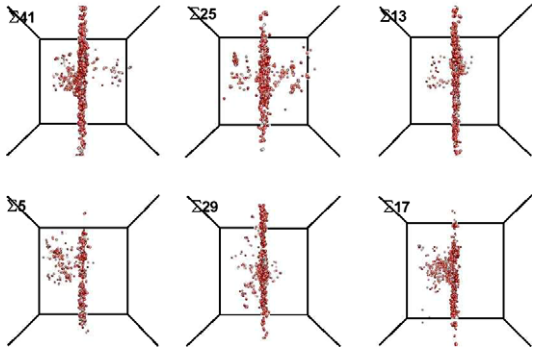

Fig. 11. Snapshots of the spatial distribution of point defects in the different GBs after a displacement cascade initiated at 10 keV. The interfaces are located in the middle of the boxes.

This is due to the fact that the simulation is done with a constant number of atom and no dumbbell has been found. A closer analysis of these numbers gives more details on how the point defects are distributed. The difference between the number of defects in the GB core regions and the total number of defects is still higher than the total number of defects found in monocrystal. On average we find: 43 uranium vacancies and 27 uranium interstitials remaining in the bulk instead of 21 for each defects in monocrystal and 165 oxygen vacancies and 122 oxygen interstitials remaining in the bulk instead of 84 for each defects in monocrystal. The number of vacancies in the bulk is significantly higher than the number of interstitials while the number of interstitials in the GB core region is higher than the number of vacancies in the same region. This could be explained by the fact that during the collision sequence, atoms which are displaced over long distances toward the GB create vacancies in the bulk and are trapped in interstitial positions at the interface.

The spatial repartition of the point defects created at the end of cascades with different GB geometries is compared in Fig. 11. In all the cases, there is a concentration of point defects at the GB, which represents the majority of the point defects created. However, differences occur between the small GBs with misorientation angles (Σ41 and Σ25) whose pre-existing defects at the interface are made of edge dislocations and the other GBs whose pre-existing defects mainly are made of vacancies. For the small angle GBs, the defects are distributed in both crystals and at the interface whereas for the others, the defects are located mainly in the left crystal near the interface where the PKA is initialized. This confirms that the collision sequences seem to be stopped by the GBs. Only few atoms cross this barrier and create few point defects in the right crystal. The role and the nature of pre-existing defects along the GB are then very important for the cascade evolution.

5. Conclusions

Several molecular dynamics simulations have been carried out in order to study the influence of grain boundaries on the primary damage created by a displacement cascade. Six symmetrical tilt grain boundaries with different misorientation angles have been studied. After relaxation the grain boundary structure of the small misorientation angles (Σ41 and Σ25) is composed of edge dislocations. For the other angles, the grain boundary structure is composed of vacancy layer. In the particular case of Σ5 vacancy layer forms a triangular-like pattern which corresponds to the pattern found in yttria-stabilized cubic-zirconia.

The study of displacement cascades initiated with small energy (10 keV) shows numerous point defects at the grain boundary interface. Moreover, the total number of defects found in the bulk at the end of the cascades is higher than the one found for the cascades initiated with the same energy in monocrystals. For grain boundaries with vacancy defects at their interface (i.e. misorientation angle higher than 20°), the cascade morphology presents an asymmetry between the two halves of the bicrystal and point defects are only found at the interface and in one of the crystals. The interface acts like a sink which traps the least energetic atoms. The role of the pre-existing defects at the interface is then of great importance for the displacement cascade sequences.

References

[1] L. Van Brutzel, M. Rarivomanantsoa, D. Ghaleb, J. Nucl. Mater. 354 (2006) 28.
[2] L. Van Brutzel, M. Rarivomanantsoa, J. Nucl. Mater. 358 (2006) 209.
[3] H.J. Matzke, J.L. Whitton, J. Phys. 44 (1966) 995.
[4] J.P. Stout, G.R. Lumpkin, R.C. Ewing, Y. Eyal, Matter. Res. Soc. Proc. 112 (1988) 495.
[5] M. Fayek, P. Burns, G. Yong-Xiang, R.C. Ewing, J. Nucl. Mater. 277 (2000) 204.
[6] M. Samaras, P.M. Delet, H. Van Swygenhoven, M. Victoria, J. Nucl. Mater. 351 (2006) 47.
[7] F. Javier Pérez-Pérez, R. Smith, Nucl. Instrum. and Meth. B 164&165 (2000) 467.
[8] R.W. Ballufi, A. Brokman, A.H. King, Acta Metall. 30 (1982) 1453.
[9] A.P. Sutton, R.W. Ballufi, Acta Metall. 35 (1987) 2177.
[10] R.C. Pond, D.S. Vlachavas, Proc. Res. Soc. London A 83 (1983) 1533.
[11] D. Morelon, N.D. Ghaleb, J. Delaye, L. Van Brutzel, Philos. Mag. 83 (2003) 1533.
[12] E.C. Dickey, X. Fan, J. Am. Ceram. Soc. 84 (2001) 1361.
[13] Y. Lei, Y. Ito, N.D. Browning, J. Am. Ceram. Soc. 85 (2002) 2359.
[14] S.B. Mao, Z. ad Sinnott, J. Am. Ceram. Soc. 85 (2002) 1594.
[15] T. Oyama, M. Yoshiya, H. Matsubara, Phys. Rev. B 71 (2005) 224105.
[16] C.A. Fisher, H. Matsubara, Comput. Mater. Sci. 14 (1999) 177.
[17] G. Bishop et al., J. Appl. Phys. 53 (1982) 5596.